Stationarity of extreme bursts in the solar wind

N. R. Moloney[1,2,*] and J. Davidsen[2,†]

[1]*London Mathematical Laboratory, 14 Buckingham Street, London WC2N 6DF, United Kingdom*

[2]*Department of Physics and Astronomy, University of Calgary, 2500 University Drive NW, Calgary, Alberta T2N 1N4, Canada*

(Received 1 July 2013; published 22 May 2014)

Recent results have suggested that the statistics of bursts in the solar wind vary with solar cycle. Here, we show that this variation is basically absent if one considers extreme bursts. These are defined as threshold-exceeding events over the range of high thresholds for which their number decays as a power law. In particular, we find that the distribution of duration times and energies of extreme bursts in the solar wind ϵ parameter and similar observables are independent of the solar cycle and in this sense stationary, and show robust asymptotic power laws with exponents that are independent of the specific threshold. This is consistent with what has been observed for solar flares and, thus, provides evidence in favor of a link between solar flares and extreme bursts in the solar wind.

DOI: 10.1103/PhysRevE.89.052812 PACS number(s): 89.75.Fb, 96.50.Ci, 94.05.Lk, 05.45.Tp

I. INTRODUCTION

The exact interplay between the solar wind and the Earth's magnetosphere is an open problem of considerable interest [1,2], with phenomena ranging from storm activity on short time scales [3] to possible relationships with global warming on long time scales [4,5]. As many solar wind parameters correlate with the solar cycle [6], it is natural to search for clear physical connections between geomagnetic activity and coronal processes. For example, it is known that around solar maximum the dominant interplanetary phenomenon causing intense magnetic storms are interplanetary coronal mass ejections, while coronal holes play the most important role during solar minima [7]. This dependence on the solar cycle is also reflected in the scaling of solar wind fluctuations since these fluctuations arise due to a combination of local plasma turbulence and propagating structures of coronal origin [8,9].

As solar flares—sudden powerful bursts of energy released above active regions of the sun (see, for example, Refs. [10,11] for a review)—are the most energetic events in our solar system [12], one expects that they are important for heating the solar wind [13] and, hence, to see some signature of them in the solar wind. Indeed, we showed very recently that during solar maximum solar flares and bursts in the solar wind parameter ϵ share many statistical properties including the same distribution of burst durations and energies if—and only if—one considers extreme bursts [14]. These are defined as threshold-exceeding events over the range of high thresholds for which their number decays as a power law. Since ϵ is a solar-wind proxy for the power input into the Earth's magnetosphere, the findings imply that the scaling of extreme solar flares gives rise to a clear signature in the extreme energy input into the magnetosphere.

Here, we investigate whether these findings also hold during solar minimum, when the solar activity is vastly different and one should consider the full-disk EUV/XUV solar irradiance as the driver of the solar wind [15]. Yet, we find that the solar cycle has no significant influence on the statistical properties of extreme bursts in the ϵ parameter—in sharp contrast to the behavior of nonextreme bursts. This indicates that the properties of extreme bursts are stationary (independent of solar cycle) and universal. Specifically, the distribution of burst energies follows a power law with exponent $\approx$1.6 over all scales while the distribution of burst durations is only asymptotically a power law with exponent $\approx$2.4. Both distributions are independent of the applied threshold. This is consistent with findings for soft x-ray emission in solar flares [10,16]. The distributions of time intervals between two subsequent extreme bursts, however, are markedly different between the solar wind and solar flares. We also show that qualitatively similar results hold if one considers extreme bursts in the magnetic energy density B^2, which is sometimes thought to be more directly coupled to solar flare activity than ϵ [8,13]. Finally, we provide evidence for a weak clustering of extreme bursts that can be explored for prediction.

The structure of the paper is as follows: We begin by introducing the Akasofu ϵ time series and defining extreme bursts in Sec. II. The statistical properties of extreme and nonextreme bursts as well as the time intervals between bursts are studied in Secs. III and IV, respectively. Section V compares the extreme bursts in the ϵ parameter to those of the magnetic energy density B^2. Section VI looks into the dependence structure of subsequent extreme bursts, which could serve as a predictive tool. The article concludes with Sec. VII where we also present a comparison with the statistical properties of solar flares.

II. AKASOFU ϵ PARAMETER

The Akasofu ϵ parameter [17] is a solar-wind proxy for the energy input into the Earth's magnetosphere (see [18] for a more recent discussion). In SI units it is defined as

$$\epsilon = v\frac{B^2}{\mu_0}\ell_0^2 \sin^4(\theta/2), \tag{1}$$

where v is the solar wind velocity, B is the magnetic field, $\mu_0 = 4\pi \times 10^{-7}$ is the permeability of free space, $\ell_0 \approx 7R_E$, and $\theta = \arctan(|B_y|/B_z)$. Geocentric solar magnetospheric (GSM) coordinates are used. Here, we consider the time series of ϵ

*n.moloney@lml.org.uk

†davidsen@phas.ucalgary.ca

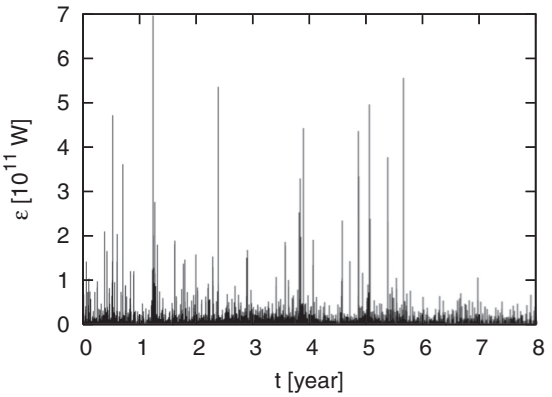

FIG. 1. Akasofu ϵ parameter derived from ACE data for the years 2000–2007.

as measured by the ACE spacecraft. The ACE spacecraft [19] orbits the Earth-Sun L1 libration point approximately 1.5×10^9 m from the Earth and monitors solar wind, interplanetary magnetic fields, and high-energy particles [20]. Specifically, for the years 2000–2007, we extracted the magnitude of the x component of the solar wind, and the y and z components of the magnetics fields, as seen respectively by the SWEPAM and MAG instruments (level 2 data) of the ACE spacecraft, all in GSM coordinates. The choice of components reflects the Poynting flux interpretation of the ϵ parameter. For the most part, measurements are available every 64 and 16 s for the wind velocity and magnetic fields, respectively. We calculated the ϵ parameter every 64 s. Since the wind velocity and magnetic field measurements are not synchronized, we linearly interpolated the magnetic field measurements towards the time of the nearest wind velocity measurement. For these 8 years the ϵ time series consisted of 3 944 700 points; see Fig. 1. Measurements for wind velocities or magnetic fields are sometimes unavailable. Approximately 9 percent of the points comprising the ϵ series are missing. As in Ref. [16], we set missing data points to the value of the last valid recording preceding them (irrespective of the size of the data gap), thereby creating plateaus of constant intensity. This minimizes artifacts associated with points missing at regular experiment-specific frequencies. We have checked that nothing changes crucially in our statistical analyses by adopting other schemes.

During the 2000–2007 observation period the solar cycle is in evidence, with greater activity in the first half of the series than in the second half. We thus split up the catalog into a solar maximum phase from 01.01.2000–31.12.2004, containing 1 972 350 points, and a solar minimum phase from 01.10.2006–31.12.2007, containing 575 101 points.

Definition of extreme bursts

As in Refs. [21–23], we define bursts in the ϵ time series as periods during which the values remain above some threshold, as illustrated in Fig. 2. Thus, the duration of a burst, t_d, is the time between a threshold upcrossing and the next threshold downcrossing. Two successive upwards crossings of a threshold give the waiting time, t_w, between subsequent bursts. Finally, the time spent below threshold is denoted by the

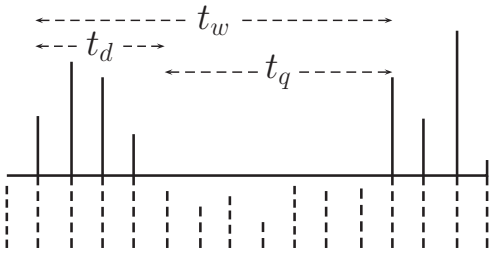

FIG. 2. Definition of waiting, duration, and quiet times, t_w, t_d, and t_q, respectively, for bursts (solid lines) exceeding a threshold, given by the horizontal line.

quiet time t_q, i.e., the time between a threshold downcrossing and the next upcrossing. The times are therefore related through $t_w = t_d + t_q$. We also consider burst sizes, given by the area of the burst above threshold, which, in the case of the ϵ series, corresponds to a quantity with units of energy. Note that our notion of bursts is different from peak-over-threshold events typically considered in extreme value theory [24].

The definition of a burst crucially depends on the chosen threshold. Raising the threshold can lead to a fragmentation of a burst into multiple bursts or to its disappearance. Lowering the threshold can lead to a merging of bursts or the creation of new bursts. Thus, the number of bursts varies with threshold. Figure 3 shows that the variation in the number of bursts is rather small for a wide range of thresholds, but a power-law decay sets in beyond $\epsilon \approx 5 \times 10^9$ W (or a little later during solar minimum). Note that the difference in the number of bursts between solar maximum and solar minimum is mainly due to the different lengths of the time series. Almost all earlier studies have exclusively focused on threshold values that were smaller than or equal to the $q = 0.9$ quantile of the distribution of ϵ values [21–23]. As Fig. 3 shows, these values are outside the power-law regime. Here, we focus predominantly on extreme bursts, which we define as those associated with

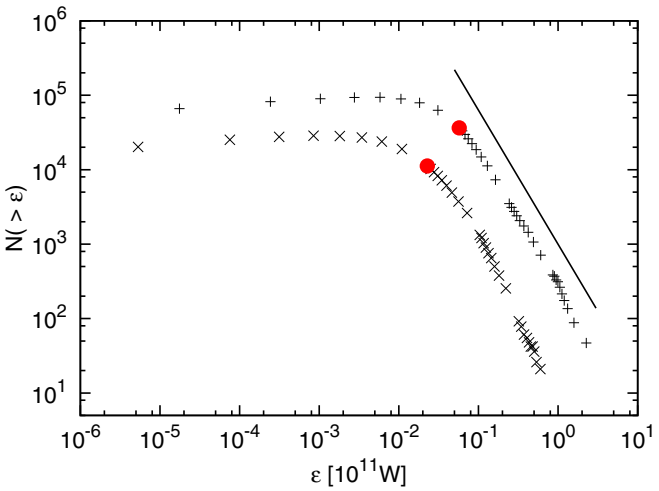

FIG. 3. (Color online) Number of events above ϵ for solar maximum (upper) and solar minimum (lower). Points corresponding to the $q = 0.9$ quantile are indicated by solid circles. The solid line has slope -1.8.

TABLE I. Thresholds for the ϵ series corresponding to quantiles $q = 0.95,0.97,0.99,0.993,0.995$.

	Solar max	Solar min	Symbol
start	01.01.2000	01.10.2006	
end	31.12.2003	31.12.2007	
threshold	0.094	0.040	+
[10^{11} W]	0.13	0.056	×
	0.24	0.10	□
	0.30	0.12	○
	0.37	0.14	△

threshold values in the power-law regime [14]. For the extreme bursts, the specific threshold values we consider are given in Table I.

III. STATISTICAL PROPERTIES OF BURSTS

A. Duration of extreme bursts

For extreme bursts in the ϵ time series during solar maximum, we have reported recently [14] that the duration time t_d follows a probability density function (PDF) described by

$$p(t_d) = \frac{\mu - 1}{t_0}\left(1 + \frac{t_d}{t_0}\right)^{-\mu}, \quad t_d \in [0,\infty). \tag{2}$$

Figure 4 and Table II show that this is also true for extreme bursts during solar minimum. In Fig. 4, the best fit using maximum-likelihood estimation of the parameters μ and t_0 is plotted for the curve corresponding to the $q = 0.993$ quantile for solar maximum and minimum, respectively. Although the function in Eq. (2) is defined for continuous values of t_d, duration time data is recorded at discrete resolution as discussed above. Thus, the maximum-likelihood function is constructed by integrating Eq. (2) over the discrete bins [25,26]. For solar maximum and minimum the p values of the fits are 0.45 and 0.58, respectively, using a G test [27] (owing to the discrete nature of the data). The width of each bin is allowed to increase to ensure that at least 20 data points fall within each bin (with the possible exception of the final bin). A χ^2 test gives similar p values. Such high p values indicate that Eq. (2) is indeed an excellent description of the data for both solar maximum and solar minimum. Table II gives the maximum-likelihood estimates of the parameters μ and t_0 for all thresholds considered. Table II also indicates that the estimates of the parameters in Eq. (2) for different thresholds are statistically indistinguishable during both solar maximum and minimum. This implies that the duration time distribution of extreme bursts are independent of the choice of the threshold. Moreover, there is very little dependence on solar cycle. Particularly at the highest thresholds, there is no statistically significant difference between the estimated exponents μ at the 95% confidence level [43]. The functional form of Eq. (2) indicates that there is a short characteristic time scale t_0, which is of the order of the discrete sampling frequency of our time series as follows from Table II. To unambiguously establish that this time scale is indeed of physical origin, one would need a higher sampling frequency of the ϵ time series. The power-law decay of Eq. (2) for larger duration times implies that these extreme bursts show scale-invariant behavior.

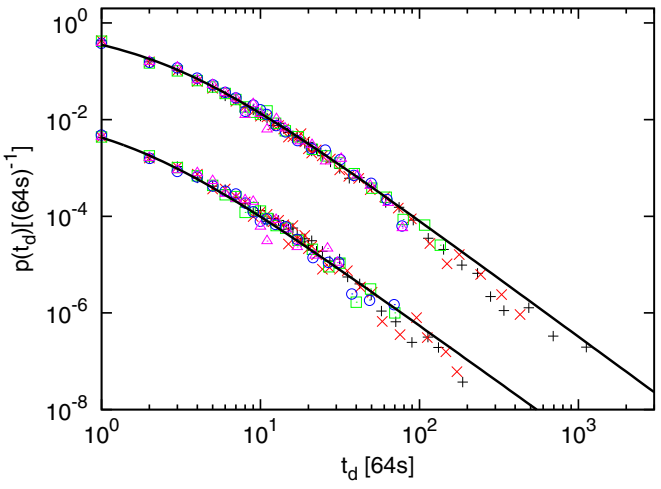

FIG. 4. (Color online) Probability density functions of the duration time of extreme bursts in ϵ during solar maximum (upper) and solar minimum (lower; displaced vertically for clarity) for thresholds at quantiles $q = 0.95,0.97,0.99,0.993,0.995$; see Table I for the corresponding symbols. The solid lines are maximum-likelihood estimates based on Eq. (2) for $q = 0.993$ quantile data (circles), with parameters given in Table II. For presentation purposes, logarithmic binning is applied to the tails where statistics are poorer.

TABLE II. Maximum-likelihood estimates of the fitting parameters μ and t_0[64 s] for Eq. (2), describing duration time probability densities for extreme bursts in ϵ. The numbers in parentheses are maximum-likelihood error estimates giving 95% confidence intervals.

	Solar max		Solar min	
Quantile	μ	t_0	μ	t_0
0.95	2.33(5)	1.5(1)	2.5(1)	1.7(2)
0.97	2.31(6)	1.5(1)	2.5(1)	1.8(3)
0.99	2.3(1)	1.5(3)	2.6(2)	1.8(5)
0.993	2.4(1)	2.1(4)	2.4(2)	1.3(5)
0.995	2.4(2)	1.9(5)	2.5(3)	1.8(8)

B. Extreme burst sizes

It is natural to consider not just the duration of a burst, but also its size. As discussed above, we define the size of a burst as the area above threshold, which corresponds to the total energy E of the burst in the case of the ϵ time series. Figure 5 shows that the PDF of the extreme burst energies, $p(E)$, decays as a power law over many decades—independently of the threshold and for both solar maximum and solar minimum. Specifically, these distributions can be characterized by

$$p(E) = \frac{\nu - 1}{E_{\min}^{1-\nu}} E^{-\nu}, \quad E \in [E_{\min},\infty). \tag{3}$$

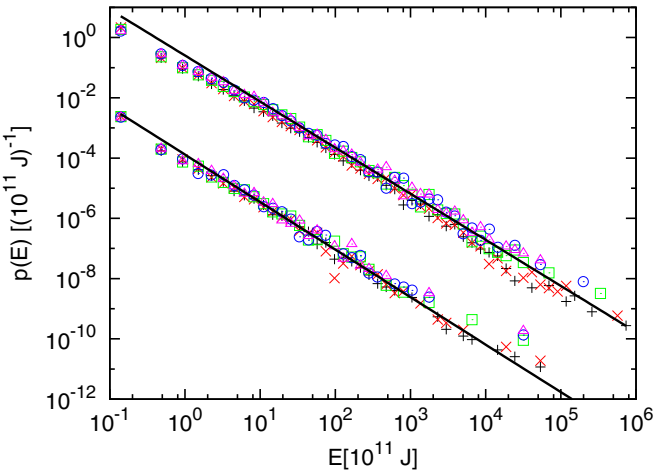

FIG. 5. (Color online) Probability density functions of extreme burst energies for ϵ during solar maximum (upper) and solar minimum (lower; displaced vertically for clarity). The solid lines are power-law fits to $q = 0.99$ quantile data (squares), with parameters given in Table III. See Table I for the meaning of symbols.

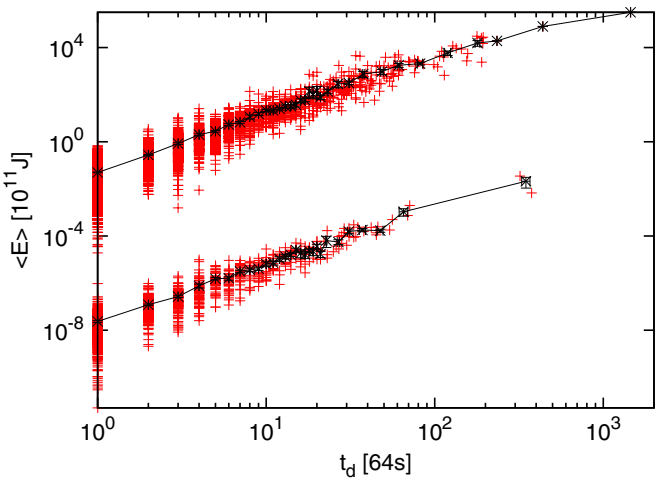

FIG. 6. (Color online) Mean extreme burst energies for ϵ (solid lines) as a function of burst duration, together with underlying scatter, for quantile $q = 0.99$ data during solar maximum (upper) and solar minimum (lower; displaced vertically for clarity).

Note that $E_{\min}$ in Eq. (3) reflects the fact that the energy of bursts of short duration is typically underestimated due to the discrete nature of the analyzed ϵ time series. The values of ν and $E_{\min}$ in Table III are maximum-likelihood estimates using Otte's implementation of the method described in Ref. [28]. Estimating the p values of these fits at the $q = 0.99$ quantile using the MATLAB code [29], we find 0.11 during solar maximum and 0.72 during solar minimum. These findings confirm that the energy distribution is scale-free with universal exponent $\nu \approx 1.55$.

In order to determine whether there is any systematic dependence between the size of a burst and its duration, in Fig. 6 we plot the scatter of burst sizes for a given duration, together with their averages, for the $q = 0.99$ quantile during solar maximum and minimum, respectively. To a good approximation, the dependence can be described by a power law, $\langle E \rangle \propto {t_d}^{\rho}$, with $\rho \approx 2.38$ for solar maximum and $\rho \approx 2.45$ for solar minimum. Moreover, the scatter around the mean energies is rather small—especially for larger durations—indicating that one can indeed associate a typical energy with an extreme burst of a given duration, $E \propto {t_d}^{\rho}$. We find that this is true for all extreme bursts independent of the threshold; see Table IV. Within statistical uncertainties, ρ is independent of the specific threshold and the solar cycle and, thus, universal for extreme bursts in ϵ.

In fact, for truly scale-invariant statistics, only two of the three exponents μ, ν, ρ are independent; see Ref. [30] for example. The transformation of probability densities $p(t_d)\,dt_d = p(E)\,dE$ gives rise to the following scaling relation:

$$\rho = \frac{\mu - 1}{\nu - 1}, \tag{4}$$

which is valid over the ranges in t_d and E corresponding to pure power laws in $p(t_d)$ and $p(E)$. Plugging in the estimated exponents for the $q = 0.99$ quantile, we find $\rho(\mu, \nu) = 2.4(3)$ for solar maximum, and $\rho(\mu, \nu) = 2.7(9)$ for solar minimum, where the uncertainty is estimated using standard error propagation. Within the statistical error bars, the derived values $\rho(\mu, \nu)$ using Eq. (4) agree very well with the directly estimated exponents. As Table IV shows, the statistical agreement is

TABLE III. Maximum-likelihood estimates of the fitting parameters ν and $E_{\min}[10^{11}\ \mathrm{J}]$ for Eq. (3), describing the extreme burst energy distribution of ϵ. Errors in brackets correspond to 95% confidence intervals. Note that the uncertainties in $E_{\min}$ (not shown) are of the same order as $E_{\min}$.

	Solar max		Solar min	
Quantile	ν	$E_{\min}$	ν	$E_{\min}$
0.95	1.59(7)	55.2	1.76(9)	19.3
0.97	1.6(1)	79.6	1.6(1)	7.7
0.99	1.53(4)	12.2	1.6(2)	4.3
0.993	1.50(6)	13.0	1.6(1)	4.1
0.995	1.48(4)	4.8	1.6(1)	3.8

TABLE IV. Estimates of ρ for $E \propto {t_d}^{\rho}$. The first set of estimates is obtained via Eq. (4), where the error is calculated by propagating the maximum-likelihood errors of μ and ν. The second set of estimates is obtained by least-squares fitting a power law to the mean extreme burst energy $\langle E \rangle$ as a function of burst duration (solid black line in Fig 6). While we also include the errors given by the least-squares fit for completeness, they vastly underestimate the true errors; see Ref. [28] for a discussion.

	Solar max	Solar min	Solar max	Solar min
Quantile	ρ [via Eq. (4)]		ρ [least-squares]	
0.95	2.2(3)	1.9(3)	2.46(2)	2.39(4)
0.97	2.2(4)	2.5(6)	2.46(3)	2.37(4)
0.99	2.4(3)	2.7(9)	2.38(4)	2.45(6)
0.993	2.8(4)	2.1(5)	2.39(4)	2.23(9)
0.995	2.9(4)	2.5(8)	2.38(5)	2.3(1)

similarly good for all other considered quantiles. This provides clear evidence for the scale invariance of sufficiently energetic and long-lasting extreme bursts.

C. Nonextreme bursts

Due to the two different regimes used to define extreme and nonextreme bursts, see Fig. 3, one might expect that there are qualitative differences in the statistical properties of extreme and nonextreme bursts. Previous studies of the ϵ time series derived from various satellite data [21–23] have concentrated on thresholds in the range $q = 0.1$–0.9, corresponding to the flat part of Fig. 3 and, thus, nonextreme bursts. For the duration time of these nonextreme bursts, the following PDF was proposed:

$$p(t_d) \propto {t_d}^{-\gamma} e^{-t_d/t_c}. \tag{5}$$

Fitting this functional form by estimating γ and t_c from the data, significant differences between different threshold values and between solar maximum and solar minimum were discovered. For example, for the $q = 0.5$ quantile γ takes the values 1.59(8) and 1.32(9) during solar maximum and solar minimum, respectively [21]. If true, this would indicate a very clear dependence of γ on the solar cycle. Unfortunately, the data were fitted to Eq. (5) using a Levenberg-Marquardt algorithm [31] that does not preserve the normalization condition of probability distributions. It has also been argued that other quantities related to ϵ exhibit variations in the burst duration distributions with solar cycle [32].

Here, we revisit the statistical properties of non-extreme bursts. Figure 7(a) reveals a clear dependence on threshold, for quantiles $q = 0.1,0.3,0.5,0.7,0.9$. Yet, this threshold dependence does not affect the functional form of $p(t_d)$ very much. In fact, a good data collapse is possible by rescaling each distribution by its mean duration time τ_d, as shown in Fig. 7(b). This is true for solar maximum and solar minimum and indicates that the threshold value predominantly influences the mean duration time for nonextreme bursts.

Although Fig. 7 gives the visual impression that the duration time distributions may be similar for nonextreme bursts during solar maximum and minimum, they are in fact statistically significantly different. We performed a Kolmogorov-Smirnov test on each solar maximum and minimum pair for quantiles $q = 0.1,0.3,0.5,0.7,0.9$, and, apart from $q = 0.9$ (for which the p value is 0.07), all others pairs have p values of the order of 10^{-4} or less. A χ^2 test gives similar results. Thus, our findings indicate that the distribution of nonextreme burst durations appears to be weakly dependent on the solar cycle, somewhat in agreement with Ref. [21].

However, in terms of the functional form of $p(t_d)$, we note that it can be modeled neither by Eq. (5) nor by Eq. (2)—as evident from Fig. 7(b). Specifically, in the former case the maximum-likelihood fitting routine (using the nlm function in the R statistical software) converges in very few cases, while in the latter case fits are obtained with extremely low p values. We also attempted to fit a power law $p(t_d) \propto t_d^{-\tilde{\mu}}$ to the tails of the distribution using again the maximum-likelihood estimator proposed in Ref. [28]. Table V gives estimates of the exponent $\tilde{\mu}$, which are approximately 2.6 and 2.8 during solar maximum and solar minimum, respectively. While these estimates give a somewhat faithful representation for the solar minimum with p values up to 0.09, for the solar maximum they should be treated with caution since the p values are rather low (less than 10^{-3}). Note also that the values of $\tilde{\mu}$ are significantly higher than the estimated values of μ for extreme bursts given in Table II, providing further evidence for the differences between extreme and nonextreme bursts.

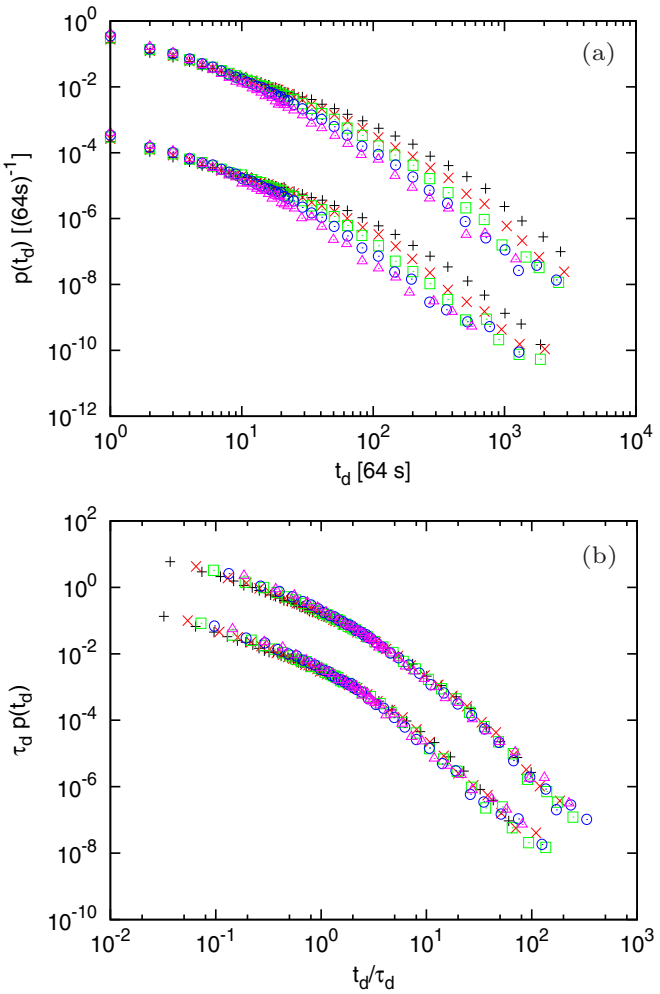

FIG. 7. (Color online) (a) Probability density functions for the duration of nonextreme bursts in the ϵ time series during solar maximum (upper set) and solar minimum (lower set; displaced vertically for clarity), for thresholds $q = 0.1,0.3,0.5,0.7,0.9$ (top to bottom). (b) As in (a) but the duration times are rescaled by their respective mean duration time τ_d.

These differences are also evident in the distribution of burst sizes. As an example, Fig. 8 shows the probability density functions for the size of bursts at quantile $q = 0.3$ during both solar maximum and minimum. While the asymptotic behavior follows Eq. (3) as for extreme bursts (see Fig. 5), there are significant differences for bursts of smaller size. In particular, the probability density function in this regime can be approximated by another power law with a (lower) exponent of about 1.1–1.2 for low quantiles $q \lesssim 0.5$, rising to about 1.3–1.4 for higher quantiles $0.5 \lesssim q \lesssim 0.9$ (independently of solar cycle). The transition point between the two power-law

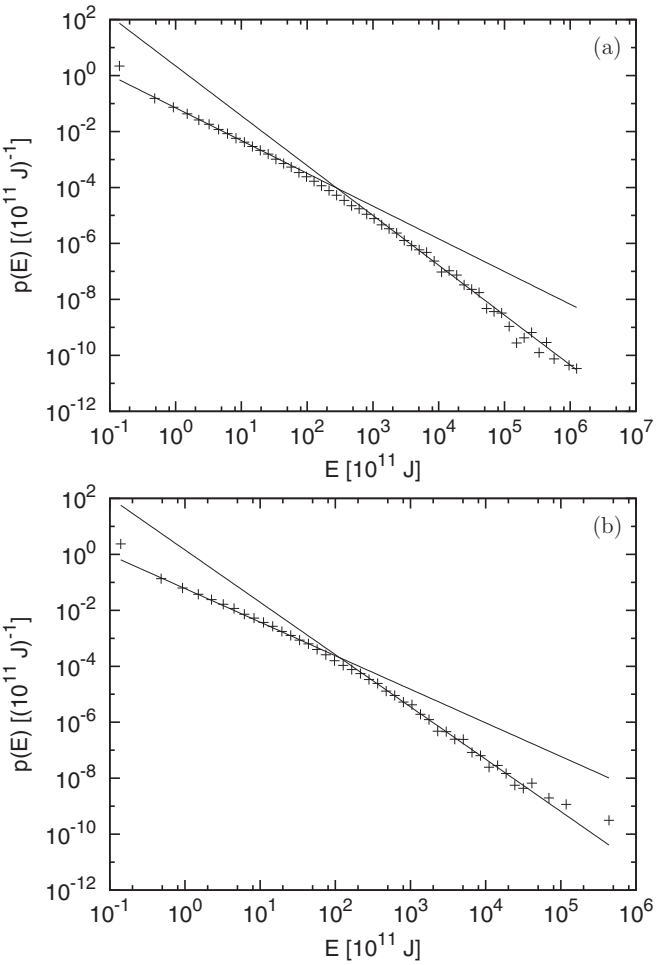

FIG. 8. Probability density functions for the size of bursts at quantile $q = 0.3$ during (a) solar maximum, (b) solar minimum. Separate power-law fits for small and large arguments are shown as solid black lines. The estimated values of the exponent characterizing the latter (asymptotic) behavior, ν, are given in Table V.

regimes moves towards lower values for larger q. This is consistent with the absence of the first power-law regime for extreme bursts.

The asymptotic behavior of the size distribution of nonextreme bursts as captured by the second power law is summarized in Table V. The maximum-likelihood estimates of the exponent ν indicate very little or no dependence on threshold and solar cycle and are only slightly higher than for extreme bursts (see Table III). p values indicate that such a power-law fit is more appropriate during solar minimum than solar maximum, although, in some cases, a power-law fit is not convincing at all. Despite this fact, the asymptotic relationship between burst size and duration, $\langle E \rangle \propto t_d{}^{\rho}$, seems to hold quite well. Figure 9 shows the case $q = 0.3$ as an example. As before (for the case $q = 0.99$), we have checked that the scatter of burst energies is sufficiently narrow for a well-defined mean value to exist.

TABLE V. Maximum-likelihood power-law estimates for the probability density functions of the duration times ($\tilde{\mu}$; see text for details) and burst sizes [ν; see Eq. (3)] for lower thresholds [10^{11} W]. The numbers in parentheses are maximum-likelihood error estimates giving 95% confidence intervals.

	Solar max			Solar min		
Quantile	Threshold	$\tilde{\mu}$	ν	Threshold	$\tilde{\mu}$	ν
0.1	1.6×10^{-5}	2.9(3)	1.8(1)	5.3×10^{-6}	2.8(3)	1.8(1)
0.3	0.0010	2.6(3)	1.8(2)	0.00031	3.0(2)	1.9(1)
0.5	0.0058	2.7(3)	1.7(1)	0.0018	2.86(9)	1.80(6)
0.7	0.018	2.6(1)	1.67(8)	0.0061	2.8(1)	1.79(8)
0.9	0.058	2.51(7)	1.61(5)	0.023	2.7(1)	1.8(1)

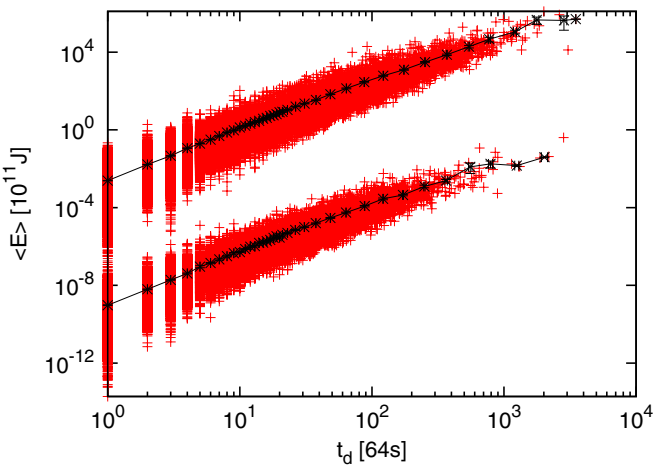

FIG. 9. (Color online) Mean burst energies for ϵ (solid lines) as a function of burst duration, together with underlying scatter, for quantile $q = 0.3$ data during solar maximum (upper) and solar minimum (lower; displaced vertically for clarity). The asymptotic scaling is characterized by $\rho \approx 2.1$ and $\rho \approx 2.3$, respectively. The least-squares estimates match well with the expected values based on Eq. (4).

IV. WAITING TIMES

A. Extreme bursts

In addition to the statistical properties of bursts themselves, the time intervals separating subsequent bursts are also of interest. Since $t_w = t_d + t_q$, the waiting time distribution could, in principle, be a nontrivial composition of duration and quiet time distributions. However, this is not the case for extreme bursts in the ϵ time series. Figure 10 shows that for quantile $q = 0.95$, to a good approximation, the waiting and quiet time distributions are similar with differences only appearing for short times. This behavior is a consequence of the fact that extreme bursts are relatively localized. For example, for quantile $q = 0.95$ the mean duration time $\tau_d \approx 5.5$ min is much smaller than the mean quiet time $\tau_q \approx 104.4$ min. Moreover, the duration time of an extreme burst has little effect on the subsequent quiet time (see Sec. VI for an analysis of possible correlations). Thus, $t_w \approx t_q$ for sufficiently large values and the duration time only leads to deviations for small values. We find that this is generally true for extreme bursts independent of the threshold and the solar cycle. Thus, we

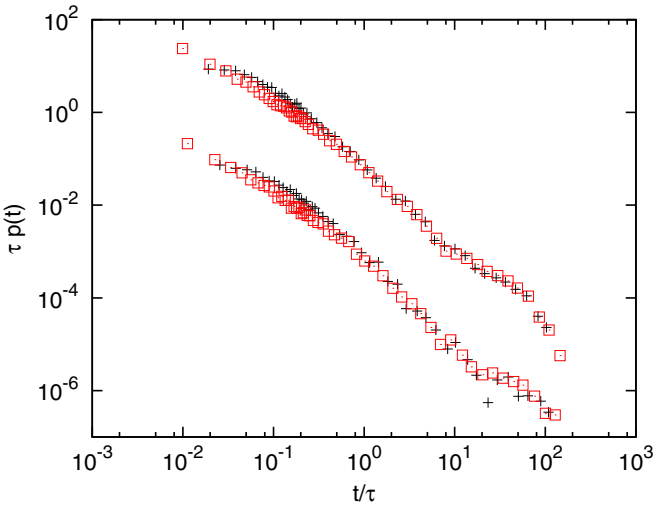

FIG. 10. (Color online) Waiting (crosses) and quiet (squares) time probability densities during solar maximum (upper) and solar minimum (lower; displaced downwards for clarity) rescaled by mean waiting/quiet time $\tau_{w,q}$, for quantile $q = 0.95$.

focus on waiting times in the following but we obtain very similar results for quiet times.

In sharp contrast to the duration time distribution of extreme bursts, both the waiting and quiet time distribution are not independent of threshold and solar cycle. As Fig. 11 shows, the distributions develop a shoulder with increasing threshold at some characteristic time scale which depends on solar cycle:

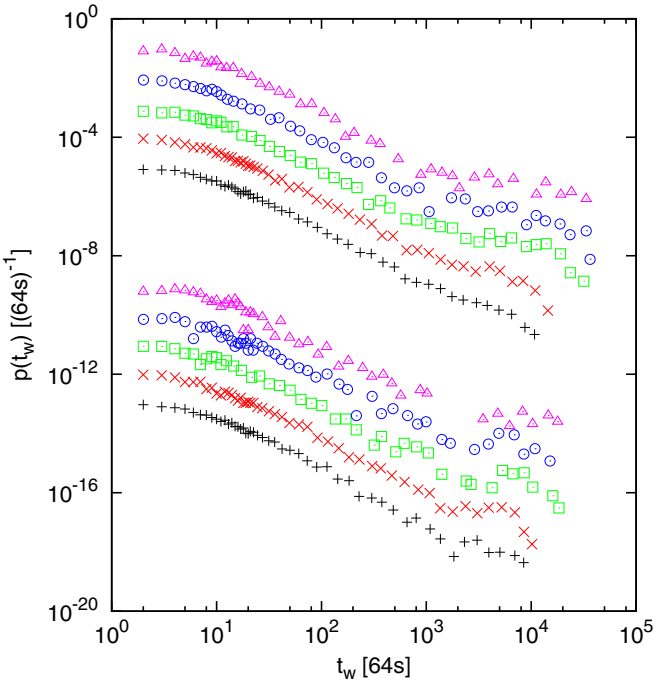

FIG. 11. (Color online) Probability density functions of waiting times between subsequent extreme bursts in ϵ during solar maximum (upper set) and solar minimum (lower set) for thresholds $q = 0.95, 0.97, 0.99, 0.993, 0.995$. See Table I for the meaning of symbols. Curves have been displaced vertically for clarity.

$t_c \approx 500$ min for solar maximum, and $t_c \approx 2000$ min for solar minimum. We have checked whether the characteristic time depends on periods of intense activity by conditioning the second waiting time in an adjacent pair of waiting times on the first. Specifically, if the first waiting time is less than the mean waiting time for the whole catalog, then the second waiting time contributes to a "high activity" subset, else it contributes to a "low activity" subset. We find no discernible differences in the waiting time distributions between the two subsets. This indicates that the characteristic time scale has rather a solar origin and is likely not a consequence of the local plasma turbulence in the solar wind. However, it seems unrelated to the dynamics of solar flares as a direct comparison shows [14].

Characteristic time scales for similar (but not identical) observables have been documented in the literature. For example, in studies of magnetic field changes and spatial correlation functions in solar wind turbulence during solar maximum, estimates of correlation times (typically attributed to the underlying magnetohydrodynamic turbulent cascade)

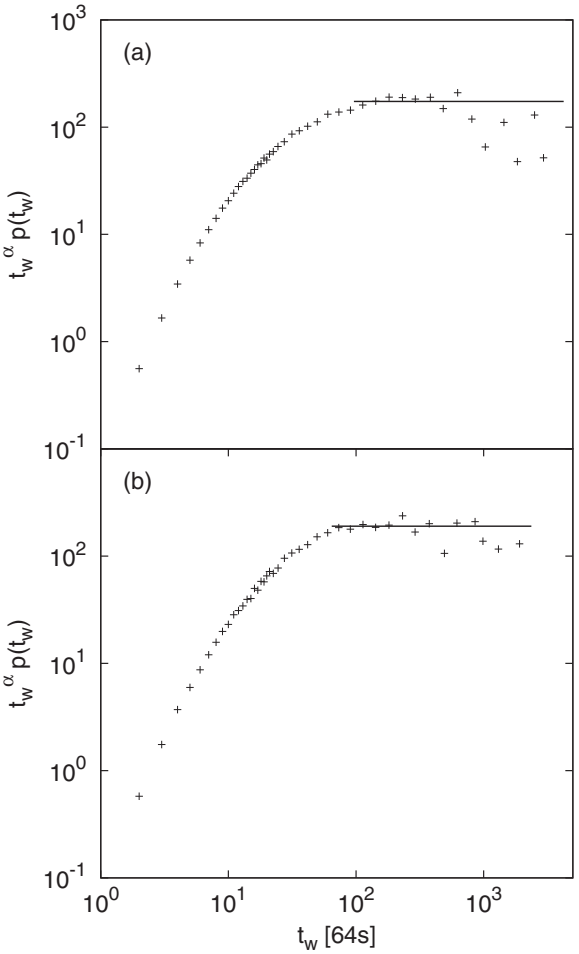

FIG. 12. Transformed probability density functions for the waiting time of bursts at quantile $q = 0.5$ during (a) solar maximum, (b) solar minimum. Each function has been multiplied by $t_w{}^{\alpha}$, where α is the maximum-likelihood estimate of the exponent of a fitted power law; see text for details. The fits are indicated by the solid black lines.

are in the range 50–600 min [33,34]. This time scale is broadly consistent with the monoscaling window of ϵ increments [35–37], which breaks down in the range 300–600 min.

B. Nonextreme bursts

At lower thresholds, the shoulder and the associated characteristic time scale in the waiting time distribution disappear altogether. While one could expect that the distributions are well described by power laws in this case [23], this is typically not so. The majority of maximum-likelihood fits suffer from very low p values (less than 10^{-2}). This is especially true during solar maximum. Figure 12 illustrates these significant deviations from power-law behavior for $q = 0.5$, where the distributions have been transformed in order to expose a possible power-law tail as a horizontal line. The solid lines represent maximum-likelihood fits to a power-law asymptote. The estimated exponents are $\alpha = 2.8(2)$ for solar maximum (fitting beyond $t_{w;\min} = 96[64\,\mathrm{s}]$) with $p < 10^{-4}$, and $\alpha = 2.81(9)$ for solar minimum (fitting beyond $t_{w;\min} = 65[64\,\mathrm{s}]$) with $p = 0.12$. Unlike in the case of duration time distributions [see Fig. 7(b)], the waiting time distributions of nonextreme bursts for different thresholds cannot be collapsed onto each other after rescaling by their respective mean waiting times (not shown). We obtain qualitatively similar results for the quiet times. Note that, for nonextreme bursts, waiting times can be very different from quiet times since the duration time is generally no longer negligible.

V. EXTREME BURSTS IN B^2

To investigate whether our findings for extreme bursts in the solar wind are specific to the chosen observable ϵ, we also consider the time series of magnetic energy density B^2 alone. This also allows us to study the connection between solar flare activity and the solar wind in more detail since B^2 is thought to be a more direct indicator of solar flare activity than ϵ—the solar wind velocity v is thought to be only weakly related to solar flare activity [8,13]. In fact, we find no *qualitative* differences between the duration, size, or waiting time statistics of extreme bursts in ϵ and B^2 as we show in the following. The absence of variations in the statistics of extreme bursts with respect to solar cycle and chosen threshold is in sharp contrast to other properties of the B^2 time series that do vary with solar cycle [8,13].

As for ϵ, we find that the variation in the number of events above a given threshold with the value of the threshold exhibits two distinct regimes for B^2. This follows from Fig. 13 and allows us to define extreme and nonextreme bursts as before. In contrast to ϵ, however, the number of events decays faster than a power law during solar minimum. Just as for ϵ, we focus on extreme bursts in B^2. The thresholds for these extreme bursts are give in Table VI.

TABLE VI. Thresholds for the B^2 series corresponding to quantiles $q = 0.95,0.97,0.99,0.993,0.995$.

	Solar max	Solar min	Symbol
start	01.01.2000	01.10.2006	
end	31.12.2003	31.12.2007	
threshold	0.15	0.067	+
[10^{-15} T^2]	0.20	0.088	×
	0.37	0.14	□
	0.45	0.16	◯
	0.56	0.19	△

Figure 14 shows that the duration times of extreme bursts in B^2 follow a probability density function that can be described by Eq. (2). The estimated parameters for Eq. (2) are collected in Table VII. Evidently, they are essentially independent of both threshold and solar cycle. However, the exponent μ differs markedly between ϵ and B^2 as a comparison with Table II shows. The much smaller value of μ in the case of B^2 indicates

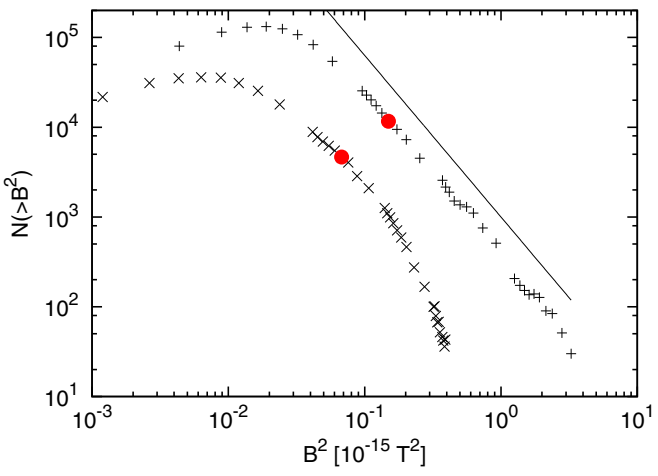

FIG. 13. (Color online) Number of events above B^2 for solar maximum (upper) and solar minimum (lower). Points corresponding to the $q = 0.95$ quantile are indicated by solid circles. The solid line has slope −1.8.

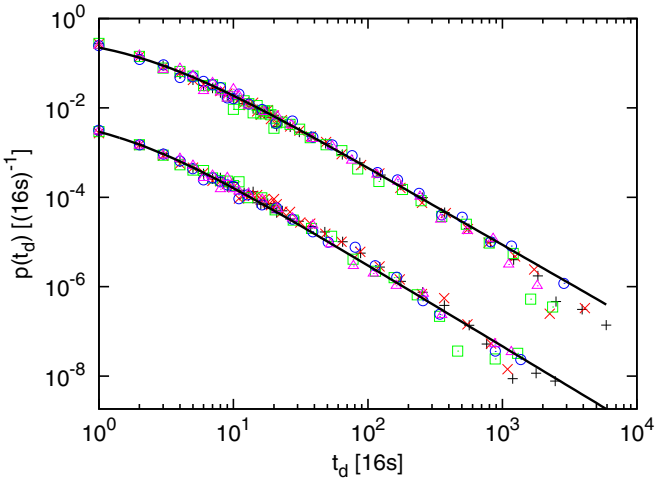

FIG. 14. (Color online) Probability density functions for the duration time of extreme bursts in B^2 during solar maximum (upper) and solar minimum (lower; displaced vertically for clarity). The solid lines are fits to the functional form given by Eq. (2) for $q = 0.993$ quantile data (circles). The estimated parameters are given in Table VII. See Table VI for the meaning of all other symbols.

TABLE VII. Maximum-likelihood estimates of the fitting parameters μ and t_0[16 s] for Eq. (2), describing the probability density function for the duration time of extreme bursts in B^2.

	Solar max		Solar min	
Quantile	μ	t_0	μ	t_0
0.95	1.72(2)	1.3(1)	1.82(4)	1.8(2)
0.97	1.74(3)	1.5(2)	1.78(5)	1.6(3)
0.99	1.76(5)	1.5(3)	1.9(1)	1.7(4)
0.993	1.73(7)	1.8(4)	1.8(1)	1.3(4)
0.995	1.79(8)	1.9(5)	1.9(1)	1.7(6)

TABLE VIII. Maximum-likelihood estimates of the fitting parameters ν and $s_{\min}[10^{-12}\,\mathrm{T}^2\,\mathrm{s}]$ using the same functional form as Eq. (3), describing the probability density function of extreme bursts sizes in B^2.

	Solar max		Solar min	
Quantile	ν	$s_{\min}$	ν	$s_{\min}$
0.95	1.40(9)	47.8	1.4(1)	2.7
0.97	1.34(4)	3.4	1.5(3)	13.8
0.99	1.33(4)	3.1	1.4(1)	1.1
0.993	1.35(9)	13.2	1.4(1)	1.2
0.995	1.34(7)	4.5	1.38(9)	0.1

that extreme bursts of large duration are more common than for ϵ. The estimated values of t_0 are again close to the discrete sampling time of the data, which is four times smaller for the B^2 series. This suggests that t_0 does not have a physical origin.

Figure 15 plots the probability density functions of extreme burst sizes, $p(s)$. Asymptotically, power-law decays are visible over many decades indicating that Eq. (3) is a good description. The fitted exponents ν are essentially independent of threshold and solar cycle; see Table VIII. While this coincides with the findings for ϵ, the value of ν is again different between ϵ and B^2 as follows from a comparison with Table III. In addition to the smaller value of ν, the observed range of extreme burst sizes is much bigger for B^2.

As for ϵ, we find that there is typically a correspondence between the size of an extreme burst and its duration. Figure 16 plots the scatter of burst sizes s for a given duration, together with their averages, for the $q = 0.99$ quantile during solar maximum and solar minimum. To a good approximation, the dependence is power law, $s \propto {t_d}^{\rho}$, with least-squares fits giving $\rho \approx 2.43$ for solar maximum and $\rho \approx 2.46$ for solar minimum—in *quantitative* agreement with the values for ϵ.

Table IX indicates, once again, little dependence on either threshold or solar cycle. Following the same analysis as for ϵ, an alternative estimate of ρ for B^2 bursts is provided by Eq. (4). Plugging in the estimated exponents for the $q = 0.99$ quantile, we find $\rho(\mu,\nu) = 2.3(3)$ for solar maximum and $\rho(\mu,\nu) = 2.1(7)$ for solar minimum, where the uncertainty is estimated using standard error propagation. Table IX includes estimates of $\rho(\mu,\nu)$ obtained in this way, as well as least-squares estimates for comparison. The quantitative agreement in ρ between the ϵ and the B^2 series indicates that by changing the observable the duration of an extreme burst is "transformed" in a similar way to its size.

The waiting time distributions for B^2 show the same features as for ϵ (results not shown), namely, little dependence on solar cycle, but a threshold-dependent shoulder in the distribution that develops for quantiles $q \gtrsim 0.9$ at a characteristic time of approximately 500–600 min. In contrast to ϵ, however, there is no clear difference in this characteristic time between solar maximum and solar minimum. This dependence on the specific observable suggests that the origin of the characteristic time is rather nontrivial.

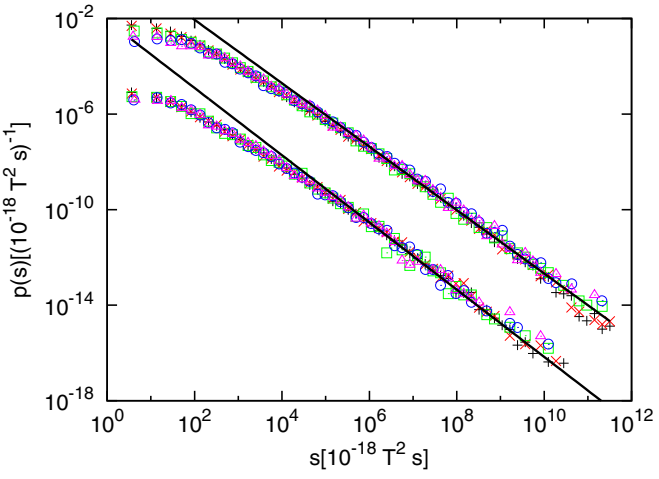

FIG. 15. (Color online) Probability density function for extreme burst sizes in B^2 during solar maximum (upper) and solar minimum (lower; displaced vertically for clarity). The solid lines are power-law fits according to Eq. (3) to $q = 0.99$ quantile data (squares). The estimated parameters are given in Table VIII. See Table VI for the meaning of symbols.

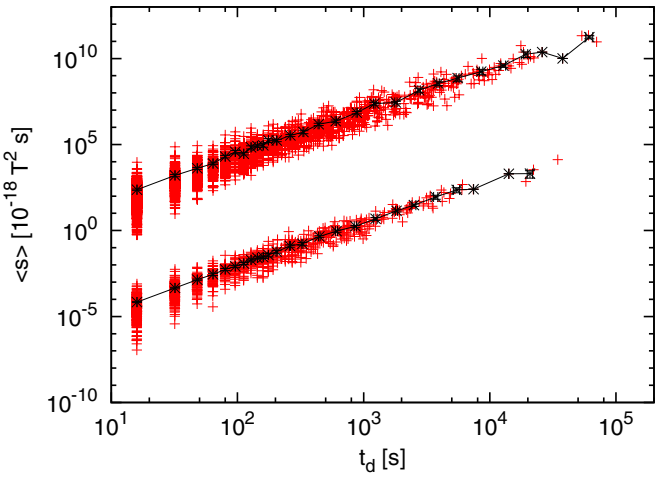

FIG. 16. (Color online) Mean extreme event sizes for B^2 (solid lines) as a function of event duration, together with underlying scatter, for quantile $q = 0.99$ data during solar maximum (upper) and solar minimum (lower; displaced vertically for clarity).

TABLE IX. Estimates of ρ for $s \propto t_d{}^{\rho}$. The first set of estimates is obtained via Eq. (4), where the error is calculated by propagating the maximum-likelihood errors of μ and ν. The second set of estimates is obtained by least-squares fitting a power law to the mean extreme burst size as a function of burst duration (solid black line in Fig. 16). Note again that the errors obtained by least-squares fitting significantly underestimate the true errors.

Quantile	Solar max ρ [via Eq. (4)]	Solar min ρ [via Eq. (4)]	Solar max ρ [least-squares]	Solar min ρ [least-squares]
0.95	1.8(4)	2.0(5)	2.49(2)	2.46(2)
0.97	2.2(3)	1.6(8)	2.52(1)	2.46(3)
0.99	2.3(3)	2.1(7)	2.43(4)	2.46(3)
0.993	2.1(6)	1.9(7)	2.45(2)	2.43(3)
0.995	2.4(5)	2.3(7)	2.42(3)	2.43(3)

VI. DEPENDENCIES BETWEEN EXTREME BURSTS

In addition to the waiting or quiet times between subsequent extreme bursts, another important characteristic is dependencies between bursts. We first consider the influence of burst size on the size of the subsequent extreme burst. Figure 17 shows the average logarithmic size of an extreme burst E_2 following an extreme burst of size of E_1, together with underlying scatter, for the $q = 0.95$ quantile during solar maximum. The plot indicates a weak tendency for subsequent burst sizes to be larger than average if the preceding burst is also higher than average. Conversely, subsequent bursts tend to be lower than average when proceeded by a burst that is also lower than average. This behavior is in keeping with the intermittent nature of the solar wind, having regimes of high and low activity. The same qualitative behavior is seen during solar minimum in Fig. 18. This weak clustering of the sizes of extreme bursts could be explored for the prediction of future burst sizes.

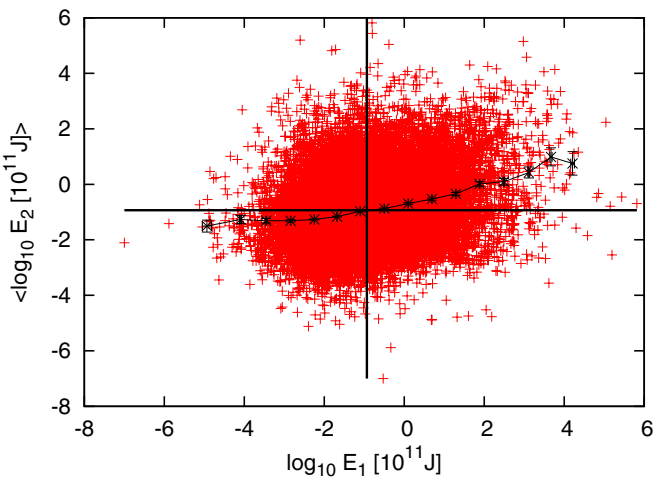

FIG. 17. (Color online) Logarithmic mean of the burst size E_2 following a burst of size E_1 (solid line), together with underlying scatter, for quantile $q = 0.95$ during solar maximum. Error bars reflect the error in the mean. The solid horizontal and vertical lines denote the average of the logarithmic burst sizes.

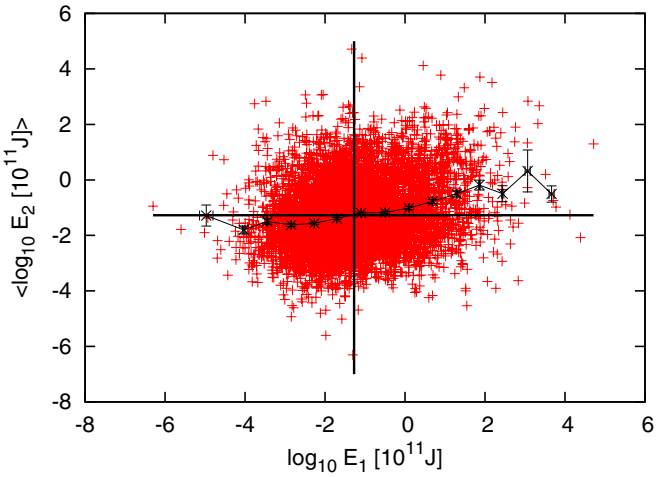

FIG. 18. (Color online) Logarithmic mean of the burst size E_2 following a burst of size E_1 (solid line), together with underlying scatter, for quantile $q = 0.95$ during solar minimum. Error bars reflect the error in the mean. The solid horizontal and vertical lines denote the average of the logarithmic burst sizes.

Figure 19 shows the average logarithmic size of a burst E following a quiet time of duration t_q, together with underlying scatter, for the $q = 0.95$ quantile during solar maximum. The plot indicates little or no relationship between burst size and quiet time, with the possible exception that long quiet times tend to be followed by bursts slightly lower than average in size. The same is true during solar minimum; see Fig. 20. In conclusion, beyond the fact that the solar wind can be in relatively active or inactive regimes (even within a solar cycle), there appears to be little dependence between burst size and the preceding burst size or quiet time, in line with results based on extreme value statistics for the ϵ series as a whole [37,38].

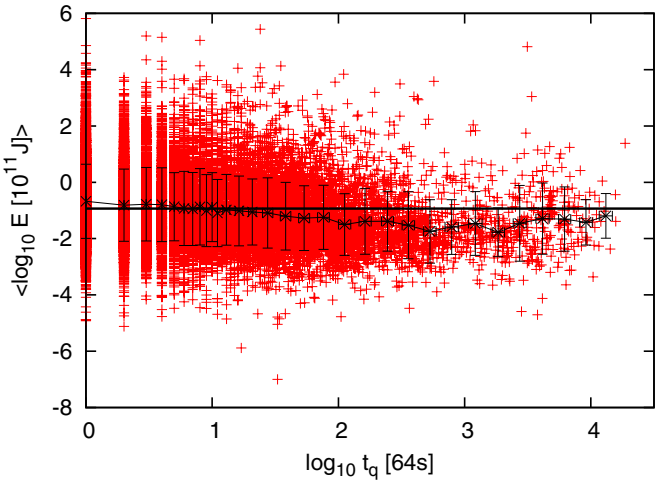

FIG. 19. (Color online) Logarithmic mean of the burst size E following quiet time t_q (solid line), together with underlying scatter, for quantile $q = 0.95$ during solar maximum. Error bars reflect dispersion in the scatter. The solid horizontal line denotes the average of the logarithmic burst sizes.

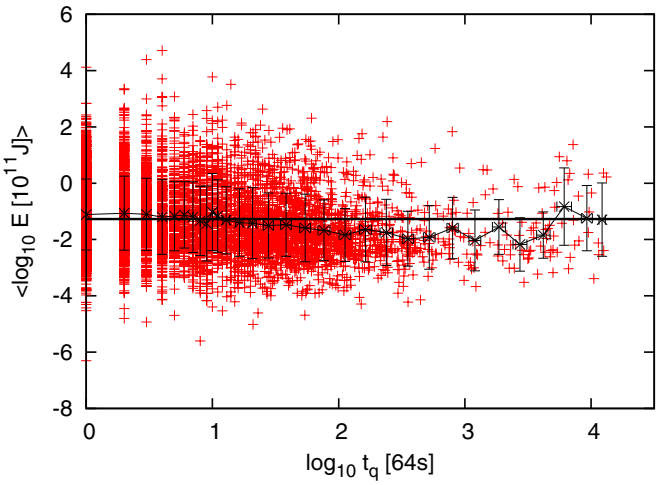

FIG. 20. (Color online) Logarithmic mean of the burst size E following quiet time t_q (solid line), together with underlying scatter, for quantile $q = 0.95$ during solar minimum. Error bars reflect dispersion in the scatter. The solid horizontal line denotes the average of the logarithmic burst sizes.

VII. DISCUSSION AND CONCLUSIONS

Our statistical analysis of extreme bursts in the solar wind provides clear evidence that the distributions of their energies and their duration times asymptotically follow power laws. These findings are in particular robust with respect to (i) the specific threshold used to define these bursts, and (ii) the specific measurement device; see the Appendix. The observed power-law behavior implies the absence of characteristic scales and further indicates the presence of scale-free properties of the underlying physical dynamics of extreme bursts. This dynamics seems to be independent of the solar cycle and stationary in this sense, but nevertheless related to solar flare activity. Specifically, defining solar flares as threshold-exceeding events, their number as a function of the threshold behaves in the same way as for bursts in the solar wind: A constant regime for small and intermediate thresholds is followed by a decaying power-law regime for high threshold [16]. This allows one to establish an analogous definition of extreme solar flares as those obtained over the range of high thresholds. More importantly, the distribution of duration times of these solar flares during both solar maximum and solar minimum follows the same functional form as that for extreme bursts in the solar wind and it is also independent of the applied threshold [16]. The estimated values of the associated power-law exponent μ are very similar to the values we obtain here for the ϵ series and in particular there is no statistically significant dependence of the exponent on the solar cycle. Measurements using a different definition of solar flares also found similar values [10]. Measurements of soft x-ray emission in solar flares showed in addition that the distribution of burst energies follows a power law with an exponent again very similar to the value of ν we obtain here for the ϵ series [10].

This quantitative agreement provides strong evidence for the direct influence of the solar activity on the statistical properties of the solar wind. Yet, it is important to realize that the agreement is "only" qualitative if one considers B^2 instead of ϵ even though the exponent ρ relating energy and duration seems to be universal. This indicates that the properties of the solar wind are qualitatively independent but quantitatively dependent on the observable chosen to characterize it, which also applies to the Poynting flux studied in [23]. The quantitative difference in the statistics between extreme bursts in B^2 and solar flares further suggests that the solar wind velocity v might be more strongly related to solar flare activity than previously thought [8,13]—at least for extreme bursts in the solar wind.

In contrast to the statistical agreement in energy and duration between extreme bursts in the solar wind and the analogously selected solar flares, the distributions of waiting times exhibit clear differences. For example, the crossover time emerging for the solar wind does not have an analog in the solar flares [16]. Nevertheless, the dependence of the crossover time on the solar cycle for ϵ but not for B^2 indicates that it might have a solar origin—unrelated to solar flares—and is partially captured by changes in the solar wind velocity v. Other differences in the distribution of waiting times are more likely to be a consequences of intrinsic properties of the local magnetohydrodynamic turbulence governing the solar wind.

While the solar cycle and the specific choice of threshold have no significant influence on the statistical properties of extreme bursts in the solar wind, our analysis shows that this is not the case if one considers nonextreme bursts. Specifically, the distribution of duration times varies with threshold predominantly by changes to the mean duration time and the distribution of energies exhibits a second power-law regime with varying exponent and crossover. Moreover, the distribution of duration times has a more complicated form than a simple power-law with exponential cut-offs for these bursts, in contrast to what has been suggested before [21]. These behaviors could be related to the underlying correlations and/or nonstationarities in ϵ as observed, for example, in the corresponding standard extreme value properties [37].

Our analysis also raises important questions in the context of the solar wind–magnetosphere interaction. While this coupling has been studied in terms of burst statistics, only thresholds below the $q = 0.9$ quantile have been considered. It will be interesting to see whether any of the recent results [21,22,39,40] need to be augmented for higher quantiles, corresponding to extreme bursts. Finally, our approach should also prove helpful for the analysis of intermittent dynamics and bursts in general; e.g., Refs. [41,42].

ACKNOWLEDGMENTS

J.D. thanks S. C. Chapman, N. W. Watkins, and V. Uritsky for helpful discussions. N.R.M. thanks A. Corral and A. Deluca for helpful discussions. We also thank the ACE SWEPAM and MAG instrument teams and the ACE Science Center for providing the ACE data, and A. Clauset and C. R. Shalizi for providing implementations for fitting power laws. This project

was financially supported by Alberta Innovates Technology Futures (formerly Alberta Ingenuity Fund).

APPENDIX: BARTOL VERSUS ADNET

Two time series for the magnetic field are available for download [20] from the ACE spacecraft, provided by the Bartol Research Institute and ADNET Systems. Thus two Akasofu ϵ time series can be constructed. The results presented here using the Bartol instrument have been cross-checked with the ADNET Systems instrument. All features are identical across the two series, except for some variation in the first decimal place for the estimated exponents reported in Tables II, III, and IV.

Figure 21 shows duration and waiting time distributions for the two ϵ series overlayed on each other for the $q = 0.99$ quantile during solar maximum. By way of comparison, a fit of the ADNET ϵ duration time distribution to the ansatz in Eq. (2) gives $\mu = 2.4(1)$ and $t_0 = 3.0(6)$. Within error bars, μ is consistent with that reported in Table II for the Bartol series.

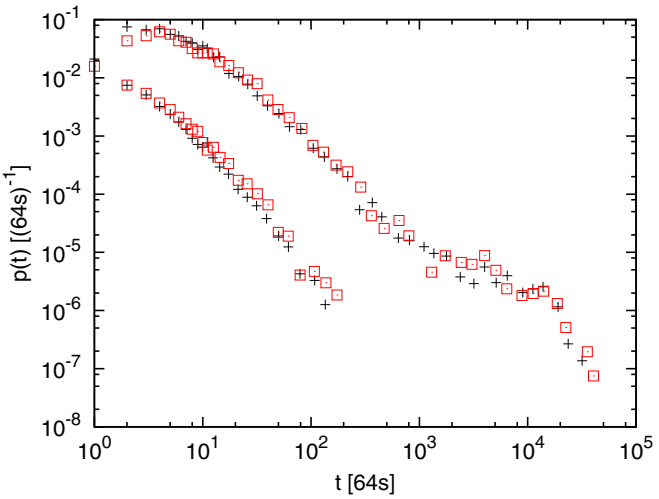

FIG. 21. (Color online) Waiting (upper) and duration (lower; displaced vertically for clarity) time probability densities for Bartol (crosses) and ADNET (squares) ϵ during solar maximum for quantile $q = 0.99$.

[1] D. N. Baker, J. Atmos. Sol. Terr. Phys. **62**, 1669 (2000).
[2] M. P. Freeman and N. W. Watkins, Science **298**, 979 (2002).
[3] W. D. Gonzalez, B. T. Tsurutani, A. L. C. Gonzalez, E. J. Smith, F. Tang, and S. I. Akasofu, J. Geophys. Res. **94**, 8835 (1989).
[4] M. Lockwood and C. Fröhlich, Proc. R. Soc. A **463**, 2447 (2007).
[5] L. J. Gray, J. Beer, M. Geller, J. D. Haigh, M. Lockwood, K. Matthes, U. Cubasch, D. Fleitmann, G. Harrison, L. Hood *et al.*, Rev. Geophys. **48**, RG4001 (2010).
[6] V. A. Osherovich, J. Fainberg, and R. G. Stone, Geophys. Res. Lett. **26**, 2597 (1999).
[7] R. D'Amicis, R. Bruno, and B. Bavassano, Geophys. Res. Lett. **34**, 5108 (2007).
[8] S. C. Chapman, B. Hnat, and K. Kiyani, Nonlinear Processes Geophys. **15**, 445 (2008).
[9] J. E. Borovsky, Phys. Rev. Lett. **105**, 111102 (2010).
[10] M. Aschwanden, *Self-Organized Criticality in Astrophysics* (Springer, Berlin, 2011).
[11] D. Hughes, M. Paczuski, R. O. Dendy, P. Helander, and K. G. McClements, Phys. Rev. Lett. **90**, 131101 (2003).
[12] M. Kretzschmar, T. D. de Wit, W. Schmutz, S. Mekaoui, J.-F. Hochedez, and S. Dewitte, Nat. Phys. **6**, 690 (2010).
[13] K. Kiyani, S. C. Chapman, B. Hnat, and R. M. Nicol, Phys. Rev. Lett. **98**, 211101 (2007).
[14] N. R. Moloney and J. Davidsen, Geophys. Res. Lett. **38**, L14111 (2011).
[15] J. Greenhough, S. C. Chapman, R. O. Dendy, V. M. Nakariakov, and G. Rowlands, Astron. Astrophys. **409**, L17 (2003).
[16] M. Baiesi, M. Paczuski, and A. L. Stella, Phys. Rev. Lett. **96**, 051103 (2006).
[17] P. Perreault and S. I. Akasofu, Geophys. J. R. Astron. Soc. **54**, 547 (1978).
[18] H. E. J. Koskinen and E. Tanskanen, J. Geophys. Res. **107**, 1415 (2002).
[19] E. C. Stone, A. M. Frandsen, R. A. Mewaldt, E. R. Christian, D. Margolies, J. F. Ormes, and F. Snow, Space Sci. Rev. **86**, 1 (1998).
[20] See http://cdaweb.gsfc.nasa.gov.
[21] J. A. Wanliss and J. M. Weygand, Geophys. Res. Lett. **34**, L04107 (2007).
[22] M. P. Freeman, N. W. Watkins, and D. J. Riley, Geophys. Res. Lett. **27**, 1087 (2000).
[23] M. P. Freeman, N. W. Watkins, and D. J. Riley, Phys. Rev. E **62**, 8794 (2000).
[24] S. Coles, *An Introduction to Statistical Modeling of Extreme Values*, Springer Series in Statistics (Springer-Verlag, London, 2001).
[25] A. M. Edwards, R. A. Phillips, N. W. Watkins, M. P. Freeman, E. J. Murphy, V. Afanasyev, S. V. Buldyrev, M. G. E. da Luz, E. P. Raposo, H. E. Stanley, *et al.*, Nature (London) **449**, 1044 (2007).
[26] D. S. Sivia and J. Skilling, *Data Analysis: A Bayesian Tutorial* (Oxford University Press, Oxford, 2006), 2nd ed.
[27] G. R. Terrell, *Mathematical Statistics: A Unified Introduction* (Springer-Verlag, New York, 1999).
[28] A. Clauset, C. R. Shalizi, and M. E. J. Newman, SIAM Rev. **51**, 661 (2009).
[29] The MATLAB code is provided at http://tuvalu.santafe.edu/~aaronc/powerlaws.
[30] J. Wanliss and V. Uritsky, J. Geophys. Res. **115**, A03215 (2010).
[31] W. Press, S. Teulkolsky, W. Vetterling, and B. Flannery, *Numerical Recipes in C* (Cambridge University Press, 1992), 2nd ed.
[32] R. D'Amicis, R. Bruno, B. Bavassano, V. Carbone, and L. Sorriso-Valvo, Ann. Geophys. **24**, 2735 (2006).
[33] W. H. Matthaeus, S. Dasso, J. M. Weygand, L. J. Milano, C. W. Smith, and M. G. Kivelson, Phys. Rev. Lett. **95**, 231101 (2005).
[34] A. Greco, W. H. Matthaeus, S. Servidio, and P. Dmitruk, Phys. Rev. E **80**, 046401 (2009).

[35] M. L. Parkinson, Ann. Geophys. **24**, 689 (2006).
[36] N. W. Watkins, D. Credgington, B. Hnat, S. C. Chapman, M. P. Freeman, and J. Greenhough, Space Sci. Rev. **121**, 271 (2005).
[37] N. R. Moloney and J. Davidsen, J. Geophys. Res. **115**, A10114 (2010).
[38] A. Y. Schumann, N. R. Moloney, and J. Davidsen, in *Extreme Events and Natural Hazards—the Complexity Perspective*, Vol. 196 of AGU Monograph (AGU, 2012), p. 315ff.
[39] V. M. Uritsky, A. J. Klimas, and D. Vassiliadis, Geophys. Res. Lett. **28**, 3809 (2001).
[40] N. W. Watkins, Nonlinear Processes Geophys. **9**, 389 (2002).
[41] J. P. Sethna, K. A. Dahmen, and C. R. Myers, Nature (London) **410**, 242 (2001).
[42] E. Dalton, I. Clancy, D. Corcoran, A. Arshak, and G. Gooberman, Phys. Rev. Lett. **104**, 214101 (2010).
[43] Two-sided χ^2 tests between the binned duration distributions of solar max and solar min data for the same *quantile* give typical p values in the range [0.02, 0.11] for extreme bursts.